Kaban, M. K., Chen, B., Tesauro, M., Petrunin, A. G., El Khrepy, S., Al-Arifi, N. (2018): Reconsidering Effective Elastic Thickness Estimates by Incorporating the Effect of Sediments: A Case Study for Europe. - *Geophysical Research Letters*, *45*, 18, pp. 9523—9532.

DOI: http://doi.org/10.1029/2018GL079732

Geophysical Research Letters

RESEARCH LETTER
10.1029/2018GL079732

Key Points:
- Considering the effect of sediments significantly reduces estimates of the lithospheric effective elastic thickness in flat areas
- Correcting for sediments suppresses the effect of unexpressed subsurface loads and substantially reduces calculation uncertainties
- The results show a good correspondence between the effective elastic thickness variations and tectonic fragmentation of Europe

Supporting Information:
- Supporting Information S1
- Data Set S1

Correspondence to:
M. K. Kaban,
kaban@gfz-potsdam.de

Citation:
Kaban, M. K., Chen, B., Tesauro, M., Petrunin, A. G., El Khrepy, S., & Al-Arifi, N. (2018). Reconsidering effective elastic thickness estimates by incorporating the effect of sediments: A case study for Europe. *Geophysical Research Letters*, *45*, 9523–9532. https://doi.org/10.1029/2018GL079732

Received 23 JUL 2018
Accepted 29 AUG 2018
Accepted article online 4 SEP 2018
Published online 21 SEP 2018

Reconsidering Effective Elastic Thickness Estimates by Incorporating the Effect of Sediments: A Case Study for Europe

M. K. Kaban[1,2], B. Chen[3], M. Tesauro[4,5], A. G. Petrunin[1,2], S. El Khrepy[6,7], and N. Al-Arifi[6]

[1]Helmholtz-Centre Potsdam, GFZ German Research Centre for Geosciences, Potsdam, Germany, [2]Schmidt Institute of Physics of the Earth, Russian Academy of Sciences, Moscow, Russia, [3]School of Geosciences and Info-Physics, Central South University, Changsha, China, [4]Department of Mathematics and Geoscience, University of Trieste, Trieste, Italy, [5]Earth Science Department, Utrecht University, Utrecht, Netherlands, [6]Geology and Geophysics Department, King Saud University, Riyadh, Saudi Arabia, [7]National Research Institute of Astronomy and Geophysics (NRIAG), Helwan, Cairo, Egypt

Abstract In the present study we analyzed the influence of density heterogeneity in the sedimentary cover on estimates of the effective elastic thickness (EET) of the lithosphere based on a cross-spectral analysis of gravity and topography data. The fan wavelet coherence technique was employed to calculate EET for most of Europe and adjoining southern mountain belts. We employed Bouguer gravity anomalies and topography corrected for the effect of density variations within sediments. Correcting for sediments considerably suppresses the effect of unexpressed subsurface loads and substantially reduces EET estimates in areas with negligible topography variations as it was demonstrated for North Europe and East European Platform. The results show a good correspondence between the EET patterns and tectonic fragmentation of Europe and better agree with independent estimates based on the strength model of the lithosphere. Therefore, considering of the effect of sediments is essential for correct determinations of EET in flat areas.

Plain Language Summary The lithosphere is the outer rigid shell of the Earth, which overlies a viscous layer, called the asthenosphere. Knowledge of the lithosphere strength is important, for example, for understanding earthquake activity. Effective elastic thickness is a proxy for lithospheric strength and corresponds to the thickness of a homogeneous elastic plate, which deforms under loading in the same way as the real lithosphere. Thus, far, different methods used to determine this parameter have given controversial results. We demonstrate that considering the effect of sediments, which represent the soft uppermost crustal layer, provides a possibility for obtaining more consistent results. New effective elastic thickness estimates show that the European lithosphere is divided into two parts along the Trans European Suture Zone. Western Europe is characterized by predominantly low values of the effective elastic thickness and consequently weak lithosphere. In contrast, the lithosphere in Eastern Europe is much stronger. Regional variations of the effective elastic thickness obtained in this study are consistent with the tectonic partitioning of Europe with the surrounding mountain belts and help to understand ongoing tectonic processes.

1. Introduction

The strength of the lithosphere is an important factor in initiating and developing tectonic processes, deforming the lithosphere, and controlling distribution of seismicity (e.g., Watts, 2001; Willett et al., 1985). Therefore, characterizing its variation is essential for geodynamic modeling of tectonic processes. Effective elastic thickness (EET) is a useful proxy for lithosphere strength and has been used for these purposes for decades (Burov & Diament, 1995; Watts, 2001). Generally, there are two different approaches for determining EET. The first approach is based on a cross-spectral analysis of the gravity field and surface topography/bathymetry (e.g., Forsyth, 1985; Kirby, 2014). The other approach estimates the lithospheric strength based on integrative 3-D models based on seismic, gravity, and other geophysical data, which combine different parameters, such as density, composition, and temperature distributions in the crust and upper mantle (e.g., Burov & Diament, 1995; Tesauro et al., 2009).

Europe has been extensively studied using both methods; however, the obtained results are diverse in many cases (e.g., Cloetingh & Burov, 1996; McKenzie, 2003; Pérez-Gussinyé & Watts, 2005; Tesauro et al., 2009, 2012). A comparison of two studies represents the sophisticated realizations of both techniques. In the first,

Pérez-Gussinyé and Watts (2005) estimated the EET of the Europe's lithosphere based on the cross-spectral method using *Bouguer coherence* and *free-air admittance* techniques. In the second, Tesauro et al. (2009) determined variations of EET for nearly the same area using estimates of strength distribution. Although the two models presented in these studies are somewhat similar, they demonstrate several principal differences. The model of Tesauro et al. (2009) showed a division between the strong lithosphere in Eastern Europe (EET $>$ 40 km) and weak lithosphere in Western Europe (mostly $<$30 km) as clearly marked by the Trans European Suture Zone (TESZ). In contrast, in the model of Pérez-Gussinyé and Watts (2005), the strong lithosphere extended further to the West to Avalonia, reaching the British Isles.

Nearly all previous studies based on the cross-spectral analysis considered only topography and bathymetry in the surface loading model. More recently, it has been demonstrated that including sediments could significantly contribute to both gravity anomalies and surface loading (e.g., Chen et al., 2015). Especially in areas with negligible topography variations, density variations within the sedimentary layer may represent a major part of the surface load and, therefore, might bias the EET estimations based on the correlation between topography and gravity. Many recent studies provided detail information on the structure of the sedimentary cover for different regions around the Earth (e.g., Mooney & Kaban, 2010; Stolk et al., 2013; Tesauro et al., 2008; Whittaker et al., 2013). These data give the possibility to recheck previous EET estimates based on the analysis of the gravity field and topography/bathymetry. In this study, we estimate EET variations for most of Europe and the surroundings using a fan wavelet coherence method (e.g., Kirby & Swain, 2006, 2011) applied to the fields corrected for the effect of sediments. Furthermore, we compare the results obtained using the traditional analysis of the gravity field and topography with those that include density variations in the sedimentary layer.

2. Initial Data

The study area includes most of Europe, excluding the northern part and some segments of the Arabia-Eurasia collision zone (Anatolia, Zagros, the Lesser Caucasus, Alborz, and part of the Kopet Dagh; Figure 1a). In the north, the area is limited by high-resolution data on the sedimentary cover, which are taken from the EuCRUST-07 model (Tesauro et al., 2008). For topography and bathymetry, we use the ETOPO-1 (Amante & Eakins, 2008) and SRTM30_PLUS (Becker et al., 2009) models. Whenever possible, the latter employs ship-track data, which are independent of satellite altimetry directly related to the gravity field and, therefore, are more suitable for cross-spectral analysis. The initial gravity field data (free-air anomalies; Figure 1b) are based on the Eigen-6c4 model (Förste et al., 2014), which combines data from recent satellite missions and available terrestrial/airborne determinations. The maximal resolution is about 10 km (2,190 spherical harmonics degree/order); however, in the continental part, the true resolution depends on terrestrial data availability.

As previously discussed, density variations within the sedimentary layer may represent a significant part of the surface load. To implement these variations, we use several high-resolution crustal models available for the study area. The EuCRUST-07 model (Tesauro et al., 2008) provides data for most of Western and Central Europe. Further to the East, for the remainder of Europe, we employ data from Kaban (2001, 2002). For the Arabia-Eurasia collision zone and surroundings, a compilation of high-resolution data on the sedimentary layer structure is presented in Kaban, El Khrepy, and Al-Arifi (2016). The resolution of all data sets is 15′ × 15′ or higher. The combined map of sedimentary thickness in the study area is shown in Figure 1c. The described data sources also provide average density of sediments in each point of the grids. The vertically averaged values are based on density-depth relations, which are determined for each specific basin (Tesauro et al., 2008). This parameter is used to estimate the corrected or "adjusted" topography (H), which represents the total result of loading combining variations in topography/bathymetry (t) and the density heterogeneity of sediments (Chen et al., 2015):

$$\begin{aligned} &H = k{\cdot}t + S{\cdot}(\rho_s{-}2670)/2670 \\ &k = 1 \ \text{for land}, \quad k = (2670{-}1030)/2670 \ \text{for the sea}, \end{aligned} \tag{1}$$

where ρ_s is the averaged density of sediments for each point of the grid, S is the sedimentary thickness, and 2,670 and 1,030 kg/m^3, respectively, are the standard densities of topography and water. The adjusted topography is shown in Figure 1d. In the flat areas with thick sediments, one can observe substantial additional

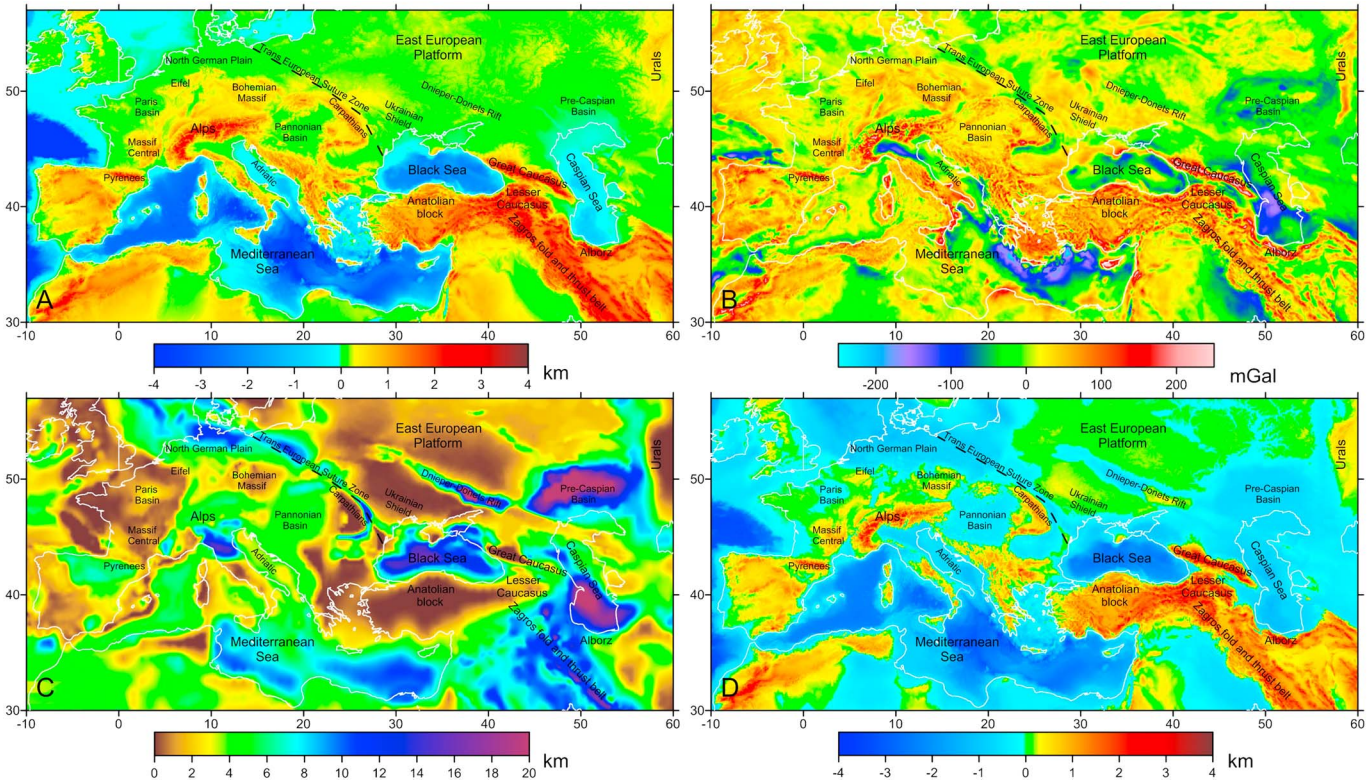

Figure 1. Study area. (a) Topography; (b) free-air gravity anomalies; (c) thickness of sediments; (d) adjusted topography corrected for the effects of water and density variations of sediments.

variations compared to the observed topography, for example, in the North German Plains, Pannonian Basin, and the East European basins (Figure 1a).

The initial gravity field (free-air gravity anomalies) is correspondingly corrected for the same effects of topography and sediments. Gravity effects from topography/bathymetry and sediments are computed and removed from the observed gravity field, which allows us to calculate standard Bouguer anomalies and residual Bouguer anomalies with the removed effect of sediments relative to the standard density of topography. These effects have been computed for all density variations within 222 km (2°) from each point taking spherical effects into account. More details on the computation technique are provided in Kaban, El Khrepy, & Al-Arifi (2016) and Kaban, El Khrepy, Al-Arifi, Tesauro, et al. (2016). Therefore, we have calculated two pairs of the fields, which are each used to calculate the EET. The first set combines the traditional Bouguer anomalies (including the correction for water) and topography with bathymetry corrected for water density. The second set of the anomalies comprises the residual Bouguer anomalies and adjusted topography, which are additionally corrected for the effect of sediments.

To calculate the EET, we also need variations of the crust-mantle boundary (Moho) because it represents the principal density contrast that provides compensation for the surface load. We use the same EuCRUST-07 model (Tesauro et al., 2008) and a recent compilation of Kaban, El Khrepy, Al-Arifi, Tesauro, et al. (2016) for the remaining area not covered by the first one. The effect of potential uncertainties in the Moho models on EET estimates is of the second order and only marginally affects them (Pérez-Gussinyé et al., 2009; Kirby & Swain, 2009).

3. Method

We employ the fan wavelet coherence method to estimate the EET (Kirby & Swain, 2004, 2006, 2011). As shown in several studies, the coherence estimates have the advantage of being much less sensitive to the unknown internal load with respect to those obtained from the admittance method (e.g., Forsyth, 1985;

Kirby & Swain, 2008). In the recent study of Chen et al. (2017), both methods were compared for EET determinations of the Antarctic lithosphere. Those authors demonstrated that, despite a general similarity of the results obtained with both methods, the coherence estimates were more robust and characterized by much less uncertainty.

The squared-real coherency (simply coherence in the following text) of the adjusted topography and residual Bouguer anomalies at scale (s) and location ($\mathbf{x}$) is determined according to Kirby and Swain (2006, 2011) as

$$\gamma^2_{obs}(s,\mathbf{x}) = \frac{\left(\mathrm{Re}\left[\left\langle B_{s\mathbf{x}\theta} H^*_{s\mathbf{x}\theta}\right\rangle_\theta\right]\right)^2}{\left\langle B_{s\mathbf{x}\theta} B^*_{s\mathbf{x}\theta}\right\rangle_\theta \left\langle H_{s\mathbf{x}\theta} H^*_{s\mathbf{x}\theta}\right\rangle_\theta}, \tag{2}$$

where H and B are the wavelet transforms of the adjusted topography and Bouguer anomalies, respectively; s and θ are the scale and azimuth of the Morlet wavelet; $< >_\theta$ is the averaging over azimuth, and $\mathbf{x}$ is the location of the calculation point in the 2-D grid. The wavelet scale (s) is related to the equivalent wave number as $k = |\mathbf{k_0}|/s$, where $|\mathbf{k_0}|$ is the central wavenumber of the wavelet. Following Kirby and Swain (2009, 2011), we determine the square of the real part of the coherency.

Using different $|\mathbf{k_0}|$ values, one can change the spatial resolution of the computed EET variations. As suggested by Kirby and Swain (2011), four values of this parameter (2.668, 3.081, 3.773, and 5.336) are primarily used for calculations; they correspond to the Morlet wavelets with the first sidelobes 1/16, 1/8, 1/4, and 1/2 relative to the central one. By increasing $|\mathbf{k_0}|$, more stable results are obtained, but the spatial resolution decreases. The low-$|\mathbf{k_0}|$ wavelets have poorer wavenumber-domain resolution which sometimes gives very large EET estimates. A reasonable choice for this parameter is particularly important for areas with high EET. As demonstrated by Kirby and Swain (2011), to resolve a high EET of more than 50–60 km, $|\mathbf{k_0}|$ should not be chosen too high.

To determine EET, the predicted coherence is estimated for a series of EET values at each point and compared with the observed one. For the predicted coherence, a *load deconvolution* method, initially introduced by Forsyth (1985), is employed. According to this method, the initial surface and subsurface loads are assumed to be uncorrelated, with the latter one assumed to be at the Moho depth. Finally, the predicted coherence is estimated as in Kirby and Swain (2011). More details on the calculated predicted coherence can be found in Audet and Mareschal (2007) and Chen et al. (2017). Because the effect of data uncertainties increases at short wavelengths, the misfit between the observed and predicted coherence is weighted by the inverse wavenumber (Kirby & Swain, 2006, 2008).

The presence of unexpressed subsurface loads can substantially bias EET estimates. To assess this effect, one can calculate the normalized squared imaginary part of the coherency for the free-air gravity anomalies ($\bar{\Gamma}^2_{F,I}$; Kirby & Swain, 2009):

$$\Gamma_F(s,x) = \frac{\left\langle G_{sx\theta} H^*_{sx\theta}\right\rangle_\theta}{\left\langle G_{sx\theta} G^*_{sx\theta}\right\rangle^{\frac{1}{2}}_\theta \left\langle H_{sx\theta} H^*_{sx\theta}\right\rangle^{\frac{1}{2}}_\theta}, \quad \bar{\Gamma}^2_{F,I} = \frac{(\mathrm{Im}[\Gamma_F])^2}{|\Gamma_F|^2}, \tag{3}$$

where $\boldsymbol{G_{sx\theta}}$ is the transform of the free-air gravity. This value should not exceed 0.5 in the vicinity of the transitional wavelength; otherwise, the results might be affected by unexpressed subsurface loads (Kirby & Swain, 2009).

4. Results

Calculated variations of the effective elastic thickness of the lithosphere for both cases (with and without considering sediments) are shown in Figures 2a and 2b. Based on a comparative analysis of different results and previous studies (Chen et al., 2015, 2017), we chose the central wavenumber of the Morlet wavelet, $|\mathbf{k_0}|$ = 3.081. This value provides reasonable stability of the results and the possibility to resolve high EET values.

The map computed without considering sediments (Figure 2a) is very close to the previous calculations of Pérez-Gussinyé and Watts (2005) and the global study of Audet and Bürgmann (2011). Similar to their

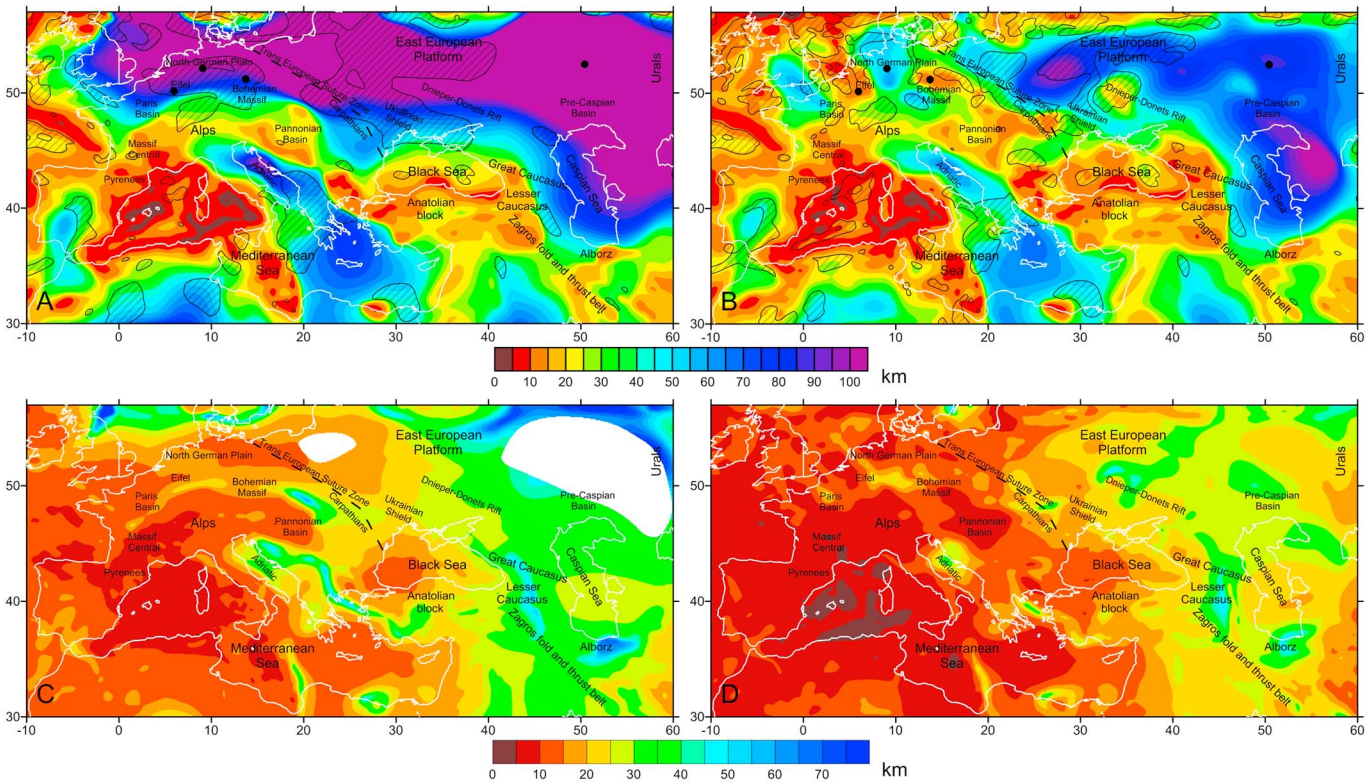

Figure 2. Variations of the effective elastic thickness (EET) of the lithosphere and their uncertainties: (a) EET estimated with the topography/bathymetry and Bouguer gravity without considering the effect of sediments. (b) EET estimated taking into account the density heterogeneity of the sedimentary cover. Black dots show the locations of coherence calculations from Figure 3. The hatched areas indicate zones where the parameter normalized squared imaginary part (equation (3)) exceeds 0.5, and the estimates of EET might be biased. (c) and (d) are the uncertainties of the EET estimations for the maps (a) and (b) correspondingly. The white zones correspond to the areas where minimum of the misfit curve is not reached.

work, we observe high values of EET in the East European Platform (EEP), which extends to Northern Europe and the British Isles. Other large-scale features are also in agreement. This confirms the consistency of the calculations based on various techniques and data sources. However, considering the effect of sediments on the gravity field and surface topography significantly changes the result in areas where the topography variations are negligible and density variations within the sedimentary cover dominate (Figure 2b). In these areas, the new EET estimates are substantially reduced compared to the previous results. The main changes are generally observed in the flat areas of Northern Europe and the EEP. The main differences of the new map are that high values are restricted to east of the TESZ; while the UK, France, and Germany are now characterized by much lower EET values (Figure 2a). Later, we discuss the spatial variations of the calculated EET. It is also important that consideration of the density variation of sediments reduces the areas with high values of the normalized squared imaginary part parameter, where the obtained EET estimates are less reliable, especially in areas with flat topography (40% vs. 51% for the northern parts of Europe and EEP), and reduce uncertainties of the calculated EET (Figures 2c and 2d).

To illustrate these results, we provide coherence graphs and misfit curves for several locations, in which the effect of sediments is particularly important (Figure 3). In all cases, the estimated EET decreases when the gravity effect from sediments is considered. The most pronounced decrease corresponds to Central and Northern Europe, where the estimated EET is 2–4 times less. When considering the effect of sediments, the misfit curves also show more pronounced minima. As suggested by Watts et al. (2006), possible uncertainties in the calculated EET can be estimated from the misfit curve; the lower and upper limits correspond to the misfit $\varepsilon = 1.05\ \varepsilon_{\min}$ of the minimal one. The uncertainties shown in Figure 2c and 2d represent half of the difference between the upper and lower limits. Indeed, we observe a significant reduction of this parameter when considering the effect of sediments. For most of Western Europe, potential uncertainties in the

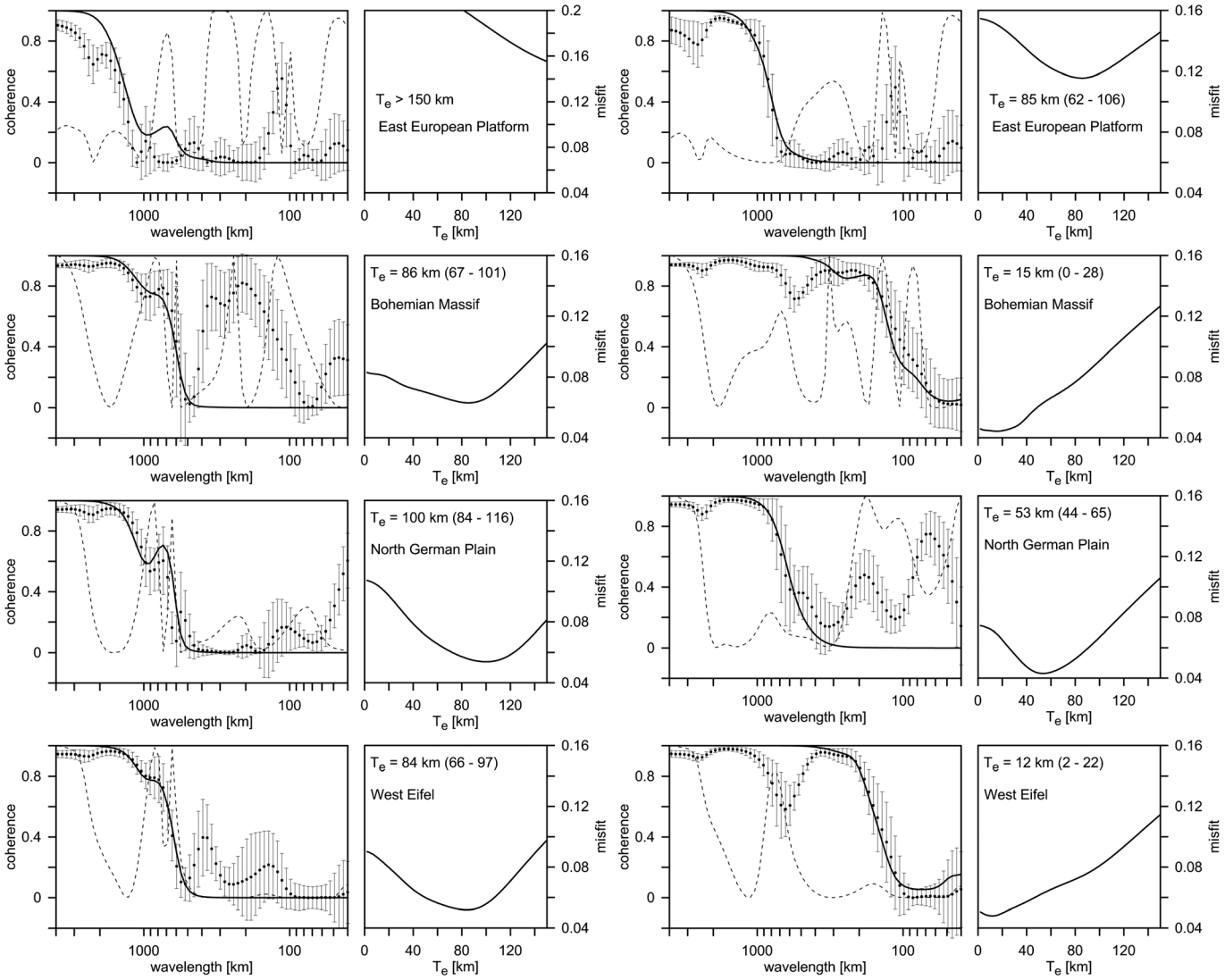

Figure 3. Coherence and misfit graphs for four points (Figure 2), $|\mathbf{k_0}| = 3.081$. Left pairs correspond to the results obtained without considering sediments, and right ones correspond to the results accounting for sediments. Dots with uncertainties are the observed coherence; the solid line demonstrates the predicted coherence for the best effective elastic thickness (T_e) with minimal misfit. The dashed line is the normalized squared imaginary part parameter. The values in parentheses are the minimum and maximum values of effective elastic thickness, which correspond to the misfit $\varepsilon = 1.05\ \varepsilon_{\min}$.

estimated EET with the sediments' correction are within ±5–10 km. For the areas with high EET, they can be larger and reach ±20–30 km, for example, in the EEP (Figure 2d). Therefore, the principal variations in the lithosphere strength (low-medium-high) can be accurately resolved.

5. Discussion

One of the basic assumptions of the cross-spectral method used to estimate EET implies that the surface and subsurface loads are uncorrelated (e.g., Forsyth, 1985). This is often not the case for sediments, which are frequently accumulated in topographic depressions. As already pointed by Artemjev and Kaban (1991), this effect can cause overestimations of the lithosphere EET. On the other hand, in relatively flat areas, the correlation between the topography and Bouguer gravity anomalies is often lost due to low-amplitude signals, which are significantly less than the unexpressed load (e.g., Figure 3, EEP). The fast decrease in correlation might be interpreted as high EET values of the lithosphere. Our analysis demonstrated that including the effect of density variations within the sedimentary cover is essential, at least when topography variations

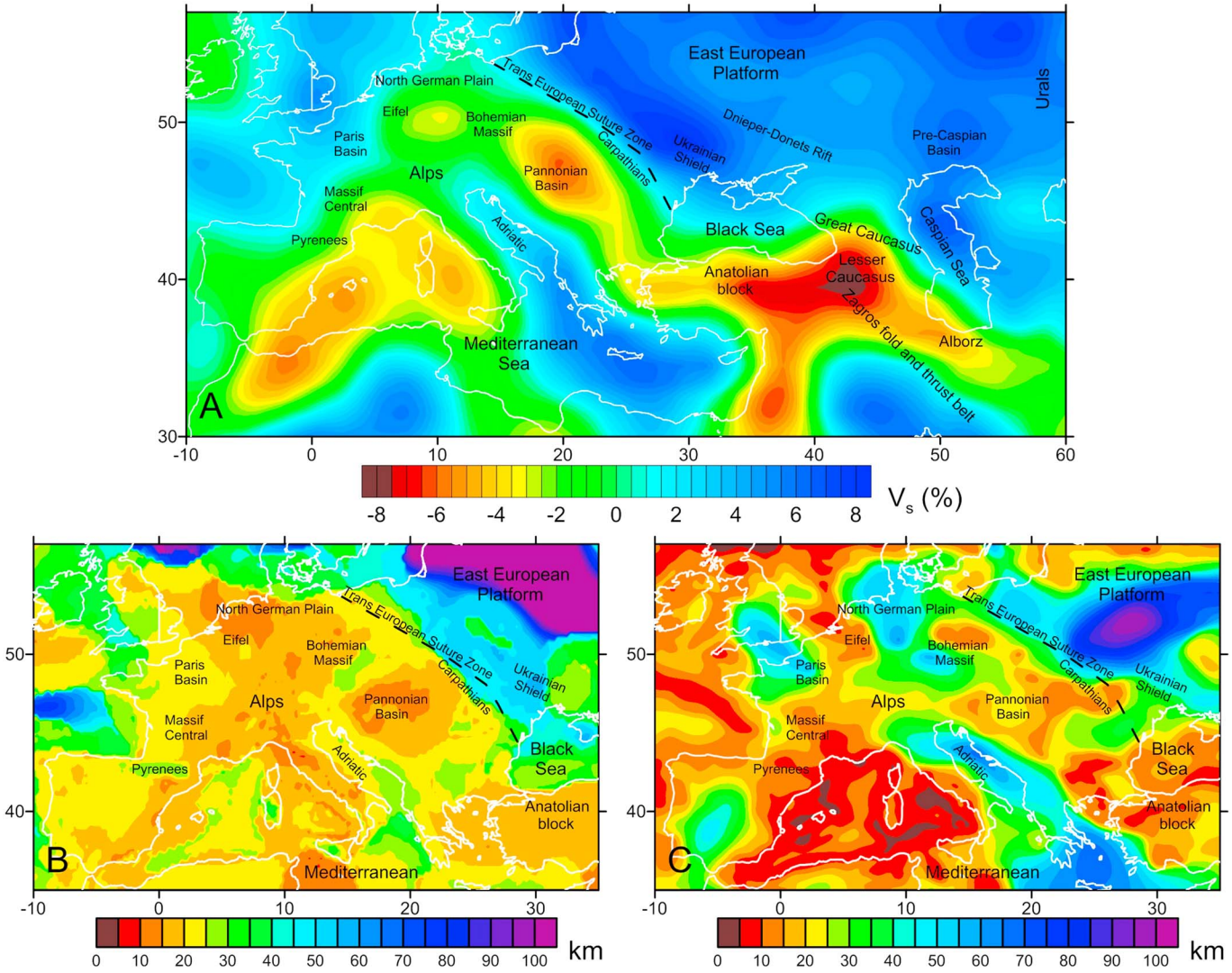

Figure 4. (a) *S* wave anomalies at a depth of 100 km (Schaeffer & Lebedev, 2013). (b) Effective elastic thickness of the lithosphere determined from the strength model of the lithosphere (Tesauro et al., 2009). (c) Effective elastic thickness estimated in the present study with the effect of sediments.

are very low. In areas with rough topography, both data sets provide similar results. In the following discussion, we analyze the EET map including the effect of sediments (Figure 2b).

To interpret the estimated EET variations, we compare them with seismic velocity anomalies in the mantle and other estimates of EET obtained from strength modeling. Seismic velocities largely depend on temperature (e.g., Cammarano et al., 2003; Goes et al., 2000), which is also one of the main factors controlling lithospheric strength (e.g., Cloetingh & Burov, 1996). *S* wave velocity variations at a depth of 100 km according to the model of Schaeffer and Lebedev (2013) are shown in Figure 4a. The EET estimates based on strength modeling are presented in Figure 4b (Tesauro et al., 2009). The last map is obtained based on an integrative analysis of thermophysical models of the crust and upper mantle.

Even if there are discrepancies in the amplitudes between the values of the new EET estimates (Figure 4c) and those obtained by Tesauro et al. (2009; Figure 4b), we can observe better correspondence of the new results in terms of distributions relatively low (<30 km) and high (>40 km) EET zones. Indeed, the new EET estimates, as those of Tesauro et al. (2009), show a distinct difference between the relatively weak lithosphere in Western Europe and strong lithosphere in Eastern Europe. This division fits the TESZ, in agreement with both the seismic tomography and strength models of the lithosphere (Figure 4). In contrast, the EET

estimates based on the topography and gravity field show very high values of EET (>100 km) for the entire area north of 50°N, which disagrees with the existing geophysical data. Furthermore, EET is also reduced in the EEP, which is divided into several domains compared to the homogeneous high EET zone in Figure 2a. The strongest lithosphere is observed in the central and eastern parts (EET > 70 km), while the southwestern part, including the Ukrainian Shield and surroundings, is characterized by values reduced to 40–50 km (Figures 2b and 4c). In the area adjoining the Dnieper-Donets Rift, EET decreases even more to about 20 km (Figure 2b).

West of the TESZ, we observe several zones characterized by EET values mostly reduced to ~10–15 km (Figure 2b), which are likely affected by recent plume activities (e.g., Ziegler & Dèzes, 2006). In addition to the Pannonian Basin and Massif Central, these are the Eifel volcanic fields and part of the Bohemian Massif, which were characterized by high EET according to the previous calculations. Most of these features are also resolved in the strength model (Figure 4b); however, the difference in the amplitude is much less. Outside of Europe, the Anatolian block and Lesser Caucasus have similar low EET values where relatively high strain rates also contribute to the reduction in lithospheric strength.

For the mountain belts, where the topography load dominates, the new results are in agreement with previous studies and show generally low EET values as for the Alps (15–25 km) and Pyrenees (~10 km). Mouthereau et al. (2013) argued that the lithospheric strength of the collision belts is inherited from the strength of the plates at the time of collision. Subsequently, despite the relatively thick lithosphere, the strength is likely reduced due to high deformation rates. Furthermore, we should consider that the resulting increase in the crustal thickness often raises the temperature at the base of the crust and thus promotes decoupling of the crust and upper mantle and, consequently, a strong reduction in EET (Burov & Diament, 1995; Tesauro et al., 2009).

The principal differences in the lithosphere EET are observed between the western and eastern parts of the Mediterranean Sea. The western part is characterized by very low EET values (5–12 km), while the eastern one has very high values (up to 67 km; Figure 2b). This division is also visible in the seismic tomography model (Figure 4a) and likely reflects differences in age and temperature. The Western Mediterranean is younger than 10 Myr and characterized by surface heat flow values >200 mW/m^2, while the Eastern Mediterranean lithosphere is older than 200 Myr and characterized by surface heat flow values <50 mW/m^2 (Davies, 2013). The Eastern Mediterranean consists of several blocks, including the Adriatic plate, which are remnants of the Neo-Tethys ocean. They formed in the late Paleozoic and formerly connected to the African plate (Garfunkel, 1998; Schattner, 2010; Schattner & Ben Avraham, 2007). The eastward decrease in EET in the Levant basin can be interpreted by the presence of a transitional type of the crust along the Eastern Mediterranean seashore (Ben-Avraham et al., 2002; Granot, 2016; Netzeband et al., 2006).

A strong difference in EET is also found between the East and West Great Caucasus. The West Great Caucasus is characterized by low EET (10–15 km), while in the East Great Caucasus, the EET reaches 50 km. Ruppel and McNutt (1990) already identified this difference based on an analysis of several profiles of the Bouguer gravity and topography. The formation of the Great Caucasus at the boundary of the strong East European plate is the likely cause of the larger EET values with respect to the other European collision belts. Several studies (e.g., Forte et al., 2014; Koulakov et al., 2012) suggest that the lithospheric root under the West Great Caucasus delaminated and sank into the mantle. The ablation of the strong part of the lithosphere led to the formation of a slab-less window filled with hot asthenospheric materials and, consequently, to a reduction of the lithospheric strength. In contrast, the colliding plates in the East Great Caucasus are coupled, and the strength of the lithosphere is high, as shown by our results.

6. Conclusions

We used Bouguer gravity anomalies and topography/bathymetry corrected for the effect of density variations within the sedimentary cover to estimate effective elastic thickness of the lithosphere for most of Europe and adjoining southern collision belts. We found that correcting for sediments considerably suppresses the effect of unexpressed subsurface loads and reduces the estimates' uncertainty. Addressing the sediment effect may principally change the estimated EET in areas with negligible variations in topography/bathymetry. In most cases, for example, in the northern part of Central Europe and the EEP, this effect causes a significant reduction in EET values. The reliability of the EET estimates is supported by their

better agreement with previous values obtained from the lithospheric strength model (Tesauro et al., 2009). Therefore, we conclude that considering of the effect of sediments is essential for correct determinations of EET in the areas with insignificant topography/bathymetry variations.

The main results for the study area are summarized as follows.

- The TESZ clearly divides areas with predominantly high values of EET (northeastern part of the study area) from those (Central and Western Europe) characterized by strongly reduced EET values.
- The EEP is also characterized by substantial variations in EET: the northeastern part shows very high values exceeding 70 km, while in the southwestern part, the EET is reduced to 40–50 km in the Ukrainian Shield and even to 20 km in the Dnieper-Donets Rift and surrounding areas.
- The lithosphere of the Mediterranean Sea is divided into two parts, the western one characterized by low EET values similar to the plume affected regions, while the eastern one, connected to the Adriatic plate, shows very high values ($>$ 55 km), reflecting differences in age and surface heat flow values.
- The EET is generally low in the collision belts in Western Europe. In contrast, the lithosphere of the East Great Caucasus shows high values ($>$50 km).

Acknowledgments
We are grateful to anonymous reviewers for their valuable comments. We acknowledge funding from German Research Foundation, SPP 2017 and PE 2167/2-1. The authors are grateful to the International Scientific Partnership Program ISPP at King Saud University for funding this research (ISPP#0052). This study is also supported by the University of Trieste (FABBR-2018), University of Utrecht, and Netherlands Research Centre for Integrated Solid Earth Sciencess (ISES-2016-434 UU-19). The calculated EET variations are provided in the supporting information.

References

Amante, C., & Eakins, B. W. (2008). *ETOPO1 1 Arc-Minute Global Relief Model: Procedures, data sources and analysis*, *National Geophysical Data Center*. Boulder, CO: NESDIS, NOAA, U.S. Department of Commerce.

Artemjev, M. E., & Kaban, M. K. (1991). Isostatic processes and intracontinental orogenesis. *Journal of Geodynamics*, *13*(1), 77–86. https://doi.org/10.1016/0264-3707(91)90031-9

Audet, P., & Bürgmann, R. (2011). Dominant role of tectonic inheritance in supercontinent cycles. *Nature Geoscience*, *4*, Q09001. https://doi.org/10.1038/ngeo1080

Audet, P., & Mareschal, J. C. (2007). Wavelet analysis of the coherence between Bouguer gravity and topography: Application to the elastic thickness anisotropy in the Canadian Shield. *Geophysical Journal International*, *168*, 287–298. https://doi.org/10.1111/j.1365-246X.2006.03231.x

Becker, J. J., Sandwell, D. T., Smith, W. H. F., Braud, J., Binder, B., Depner, J., et al. (2009). Global bathymetry and elevation data at 30 arc seconds resolution: SRTM30_PLUS. *Marine Geodesy*, *32*, 355–371. https://doi.org/10.1080/01490410903297766

Ben-Avraham, Z., Ginzburg, A., Makris, J., & Eppelbaum, L. (2002). Crustal structure of the Levant Basin, eastern Mediterranean. *Tectonophysics*, *346*(1–2), 23–43. https://doi.org/10.1016/S0040-1951(01)00226-8

Burov, E. B., & Diament, M. (1995). The effective elastic thickness (T_e) of continental lithosphere: What does it really mean? *Journal of Geophysical Research*, *100*(B3), 3905–3927. https://doi.org/10.1029/94JB02770

Cammarano, F., Goes, S., Vacher, P., & Giardini, D. (2003). Inferring upper-mantle temperatures from seismic velocities. *Physics of the Earth and Planetary Interiors*, *138*, 197–222. https://doi.org/10.1016/S00319201(03)00156-0

Chen, B., Haeger, C., Kaban, M. K., & Petrunin, A. G. (2017). Variations of the effective elastic thickness reveal tectonic fragmentation of the Antarctic lithosphere. *Tectonophysics*. https://doi.org/10.1016/j.tecto.2017.06.012

Chen, B., Kaban, M. K., El Khrepy, S, &, Al-Arifi, N. (2015). Effective elastic thickness of the Arabian plate: Weak shield versus strong platform. *Geophysical Research Letters*, *42*, 3298–3304. https://doi.org/10.1002/2015GL063725

Cloetingh, S., & Burov, E. B. (1996). Thermomechanical structure of European continental lithosphere: Constraints from rheological profiles and EET estimates. *Geophysical Journal International*, *124*(3), 695–723. https://doi.org/10.1111/j.1365-246X.1996.tb05633.x

Davies, J. H. (2013). Global map of solid Earth surface heat flow. *Geochemistry, Geophysics, Geosystems*, *14*, 4608–4622. https://doi.org/10.1002/ggge.20271

Förste, C., Bruinsma, S. L., Abrikosov, O., Lemoine, J.-M., Marty, J. C., Flechtner, F., et al. (2014). EIGEN-6C4 the latest combined global gravity field model including GOCE data up to degree and order 2190 of GFZ Potsdam and GRGS Toulouse. GFZ Data Services. https://doi.org/10.5880/icgem.2015.1

Forsyth, D. W. (1985). Subsurface loading and estimates of the flexural rigidity of continental lithosphere. *Journal of Geophysical Research*, *90*(B14), 12,623–12,632. https://doi.org/10.1029/JB090iB14p12623

Forte, A. M., Cowgill, E., & Whipple, K. X. (2014). Transition from a singly vergent to doubly vergent wedge in a young orogen: The Greater Caucasus. *Tectonics*, *33*(11), 2077–2101. https://doi.org/10.1002/2014TC003651

Garfunkel, Z. (1998). Constrains on the origin and history of the Eastern Mediterranean basin. *Tectonophysics*, *298*(1–3), 5–35. https://doi.org/10.1016/S0040-1951(98)00176-0

Goes, S., Govers, R., & Vacher, P. (2000). Shallow mantle temperatures under Europe from *P* and *S* wave tomography. *Journal of Geophysical Research*, *105*, 11,153–11,169. https://doi.org/10.1029/1999JB900300

Granot, R. (2016). Palaeozoic oceanic crust preserved beneath the eastern Mediterranean. *Nature Geoscience*, *9*(9), 701–705. https://doi.org/10.1038/ngeo2784

Kaban, M. (2001). A gravity model of the North Eurasia crust and upper mantle: 1. Mantle and isostatic residual gravity anomalies. *Russian Journal of Earth Sciences*, *3*(6), 143–163.

Kaban, M. K. (2002). A gravity model of the north Eurasia crust and upper mantle: 2. The Alpine-Mediterranean fold belt and adjacent structures of the southern former USSR. *Russian Journal of Earth Sciences*, *4*(1), 19–33.

Kaban, M. K., El Khrepy, S., & Al-Arifi, N. (2016). Isostatic model and isostatic gravity anomalies of the Arabian plate and surroundings. *Pure and Applied Geophysics*, *173*, 1211–1221. https://doi.org/10.1007/s00024-015-1164-0

Kaban, M. K., El Khrepy, S., Al-Arifi, N., Tesauro, M., & Stolk, W. (2016). Three dimensional density model of the upper mantle in the Middle East: Interaction of diverse tectonic processes. *Journal of Geophysical Research: Solid Earth*, *121*, 5349–5364. https://doi.org/10.1002/2015JB012755

Kirby, J. F. (2014). Estimation of the effective elastic thickness of the lithosphere using inverse spectral methods: The state of the art. *Tectonophysics*, *631*, 87–116. https://doi.org/10.1016/j.tecto.2014.04.021

Kirby, J. F., & Swain, C. J. (2004). Global and local isostatic coherence from the wavelet transform. *Geophysical Research Letters*, *31*, L24608. https://doi.org/10.1029/2004GL021569

Kirby, J. F., & Swain, C. J. (2006). Mapping the mechanical anisotropy of the lithosphere using a 2D wavelet coherence, and its application to Australia. *Physics of the Earth and Planetary Interiors*, *158*(2–4), 122–138. https://doi.org/10.1016/j.pepi.2006.03.022

Kirby, J. F., & Swain, C. J. (2008). An accuracy assessment of the fan wavelet coherence method for elastic thickness estimation. *Geochemistry, Geophysics, Geosystems*, *9*, Q03022. https://doi.org/10.1029/2007GC001773

Kirby, J. F., & Swain, C. J. (2009). A reassessment of spectral T_e estimation in continental interiors: The case of North America. *Journal of Geophysical Research*, *114*, B08401. https://doi.org/10.1029/2009JB006356

Kirby, J. F., & Swain, C. J. (2011). Improving the spatial resolution of effective elastic thickness estimation with the fan wavelet transform. *Computers and Geosciences*, *37*(9), 1345–1354. https://doi.org/10.1016/j.cageo.2010.10.008

Koulakov, I., Zabelina, I., Amanatashvili, I., & Meskhia, V. (2012). Nature of orogenesis and volcanism in the Caucasus region based on results of regional tomography. *Solid Earth*, *3*(2), 327–337. https://doi.org/10.5194/se-3-327-2012

McKenzie, D. (2003). Estimating T_e in the presence of internal loads. *Journal of Geophysical Research*, *108*(B9), 2438. https://doi.org/10.1029/2002JB001766

Mooney, W. D., & Kaban, M. K. (2010). The north American upper mantle: Density, composition, and evolution. *Journal of Geophysical Research*, *115*, B12424. https://doi.org/10.1029/2010JB000866

Mouthereau, F., Watts, A. B., & Burov, E. (2013). Structure of orogenic belts controlled by lithosphere age. *Nature Geoscience*, *6*(9), 785–789. https://doi.org/10.1038/ngeo1902

Netzeband, G. L., Gohl, K., Hübscher, C. P., Ben-Avraham, Z., Dehghani, G. A., Gajewski, D., & Liersch, P. (2006). The Levantine Basin—Crustal structure and origin. *Tectonophysics*, *418*(3–4), 167–188. https://doi.org/10.1016/j.tecto.2006.01.001

Pérez-Gussinyé, M., Metois, M., Fernández, M., Vergés, J., Fullea, J., & Lowry, A. R. (2009). Effective elastic thickness of Africa and its relationship to other proxies for lithospheric structure and surface tectonics. *Earth and Planetary Science Letters*, *287*(1–2), 152–167. https://doi.org/10.1016/j.epsl.2009.08.004

Pérez-Gussinyé, M., & Watts, A. B. (2005). The long-term strength of Europe and its implications for plate-forming processes. *Nature*, *436*(7049), 381–384. https://doi.org/10.1038/nature03854

Ruppel, C., & McNutt, M. (1990). Regional compensation of the Greater Caucasus mountains based on an analysis of Bouguer gravity data. *Earth and Planetary Science Letters*, *98*(3–4), 360–379. https://doi.org/10.1016/0012-821X(90)90037-X

Schaeffer, A. J., & Lebedev, S. (2013). Global shear speed structure of the upper mantle and transition zone. *Geophysics Journal International*, *194*(1), 417–449. https://doi.org/10.1093/gji/ggt095

Schattner, U. (2010). What triggered the early-to-mid Pleistocene tectonic transition across the entire eastern Mediterranean? *Earth and Planetary Science Letters*, *289*(3–4), 539–548. https://doi.org/10.1016/j.epsl.2009.11.048

Schattner, U., & Ben Avraham, Z. (2007). Transform margin of the northern Levant, eastern Mediterranean: From formation to reactivation. *Tectonics*, *26*, TC5020. https://doi.org/10.1029/2007TC002112

Stolk, W., Kaban, M., Beekman, F., Tesauro, M., Mooney, W. D., & Cloetingh, S. (2013). High resolution regional crustal models from irregularly distributed data: Application to Asia and adjacent areas. *Tectonophysics*, *602*, 55–68. https://doi.org/10.1016/j.tecto.2013.01.022

Tesauro, M., Audet, P., Kaban, M. K., Brgmann, R., & Cloetingh, S. (2012). The effective elastic thickness of the continental lithosphere: Comparison between rheological and inverse approaches. *Geochemistry, Geophysics, Geosystems*, *13*(9), 1, Q09001–18. https://doi.org/10.1029/2012GC004162

Tesauro, M., Kaban, M. K., & Cloetingh, S. (2008). EuCRUST-07: A new reference model for the European crust. *Geophysical Research Letters*, *35*(5), L05313. https://doi.org/10.1029/2007GL032244

Tesauro, M., Kaban, M. K., & Cloetingh, S. (2009). How rigid is Europe's lithosphere? *Geophysical Research Letters*, *36*(16), L16303. https://doi.org/10.1029/2009GL039229

Watts, A. B. (2001). *Isostasy and flexure of the lithosphere*. Cambridge, New York, Melbourne: Cambridge University Press.

Watts, A. B., Sandwell, D. T., Smith, W. H. F., & Wessel, P. (2006). Global gravity, bathymetry, and the distribution of submarine volcanism through space and time. *Journal of Geophysical Research*, *111*, B08408. https://doi.org/10.1029/2005JB004083

Whittaker, J. M., Goncharov, A., Williams, S. E., Müller, R. D., & Leitchenkov, G. (2013). Global sediment thickness data set updated for the Australian-Antarctic Southern Ocean. *Geochemistry, Geophysics, Geosystems*, *14*(8), 3297–3305. https://doi.org/10.1002/ggge.20181

Willett, S. D., Chapman, D. S., & Neugebauer, H. J. (1985). A thermo-mechanical model of continental lithosphere. *Nature*, *314*(6011), 520–523. https://doi.org/10.1038/314520a0

Ziegler, P. A., & Dèzes, P. (2006). Crustal evolution of western and central Europe. *Geological Society, London, Memoirs*, *32*(1), 43–56. https://doi.org/10.1144/GSL.MEM.2006.032.01.03